Techniques for Texturing Ceramic Superconductors from an Amorphous Precursor

M.J. KRAMER, R.W. MCCALLUM, L. MARGULIES, S.R. ARRASMITH, and T.G. HOLESINGER*

Ames Laboratory, Iowa State University, Ames, IA 50011

*Argonne National Laboratory, Argonne, IL 60439

Amorphous $Bi_2Sr_2CaCu_2O_8$ (Bi-2212) was crystallized under a uniaxial load of 1500 N at temperatures up to 880°C without Ag and 850°C with Ag to induce texture. Well textured samples (19 mm in diameter and 0.15 mm thick) were obtained for samples heated to within 99% of the melting temperature and quenched for samples with and without Ag. The rate limiting step for formation of the Bi-2212 from the amorphous precursor is a diffusion limited intercalation of $(SrCa)CuO_2$ into $Bi_2Sr_2CuO_6$ (Bi-2201) at T > 600°C. Samples rapidly heated to within a few degrees of the melting temperature and quenched show 20 to 30% Bi-2201 layers within the Bi-2212 structure. Annealing these samples at 850°C for > 60 h eliminates most of the Bi-2201 layers resulting in sharper superconducting transitions and higher intracrystalline critical currents with no adverse effects on grain size or texture. It is more difficult to remove the intercalations in the Ag added material.

Key words: Amorphous, Bi-Sr-Ca-Cu-O, Bi-Sr-Ca-Cu-O+Ag, TEM, texturing, XRD

INTRODUCTION

Bismuth-based superconductors (BISCCO), $Bi_2Sr_2CaCu_2O_8$ (Bi-2212) and $(Bi,Pb)_2Sr_2Ca_2Cu_3O_{10}$ (Bi-2223), have been successfully textured by partial melt processing, mechanical deformation processing, or a combination of both.[1-6] Melt processing has produced the best critical currents to date. However, it is unlikely that it will be feasible to make long textured conductors with melt processing given the slow growth rates.[7] A novel technique previously reported demonstrates that a uniaxial stress field preferentially biases the normally anisotropic grain growth to be normal to the applied load, resulting in a well textured material.[8] This technique, using an amorphous precursor, shows promise since it can form well textured material orders of magnitude faster than melt processing and shows promise to scaling-up to fabricating kilometer lengths of wire. Finely dispersing Ag in the glass and crystallizing without melting has the potential of keeping the Ag better distributed throughout the matrix.

(Received February 21, 1993)

This paper will discuss two aspects not covered previously. First, the effect of Ag addition and secondly, annealing the material to reduce or eliminate the weak-links observed in the as-textured material. These two aspects are related since the lower temperature necessary to process the Ag added glass without melting results in slower diffusion of the $(SrCa)CuO_2$ necessary to form the Bi-2212 from the Bi-2201.[9-10]

EXPERIMENTAL PROCEDURES

Material Preparation

Details of the glass formation have been presented earlier but will be summarized here for completeness.[8,11] Commercially obtained powder was sieved in a dry nitrogen atmosphere to obtain about 50 grams of agglomerated particles between 75 and 212 μm in diameter. The particles are melted in free-fall through a 1350°C vertical tube furnace back-filled with dry nitrogen to form small spherical droplets that quenched by radiative cooling. A liquid nitrogen cold trap is used to remove contaminants from the gas in the system. The resulting glass spheres were sieved

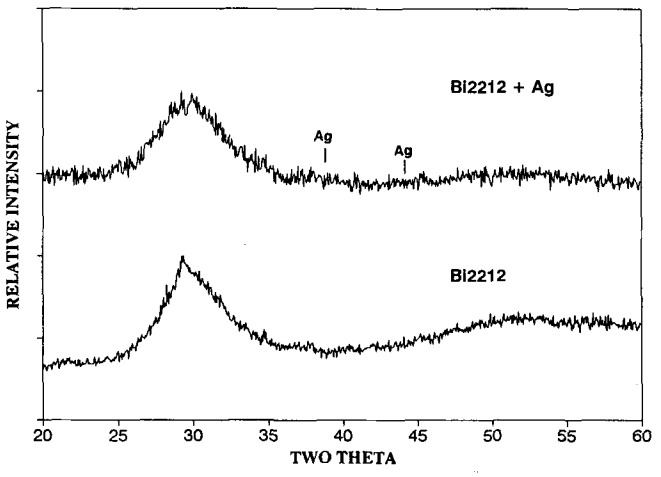

Fig. 1. X-ray diffraction pattern for the dropped BISCCO in N_2 at 1350°C and only fibers from gas jet fiberized BISCCO with 17.6 wt.% Ag.

and the fraction between 75 and 212 μm in diameter (91 wt.% recovery of the dropped material) were then micromilled under a dry nitrogen atmosphere. The powdered glass passing a 75 μm sieve was used in the texture experiments.

Silver added materials prepared in this manner resulted in a phase segregation of the Ag within the amorphous BISCCO spheres. During this relatively slow quench, the Ag had time to coarsen in the melt into particles up to 20 μm diameter. Hence, the quench rate for the drop-tube is not rapid enough to keep the silver homogeneously distributed in solution. The gas jet fiberization process[12] has a much higher quench rate and BISCCO + Ag fibers have been obtained with this technique. The initial charge had 17.6 wt.% silver added to the Bi-2212 prior to melting. This gas jet fiberization results in two particle morphologies, shot and fiber. Since the fiber should have experienced the highest quench rate, only this material was used. Inductively coupled plasma-atomic emission spectroscopy analysis revealed the nominal composition of the material to be similar to the dropped bismuth-based superconductor material $Bi_{1.93}Sr_{1.84}Ca_{0.87}Cu_{2.0}O_{7.5}$ vs $Bi_{2.09}Sr_{1.93}Ca_{1.03}Cu_{2.00}O_{7.5}$ (± 2%), yet contained only 4 wt.% Ag. Powder x-ray diffraction (XRD) shows no crystalline peaks for either technique and the position of the major Ag peak is within the noise for the fiberized material (Fig. 1). Transmission electron microscopy (TEM) using both energy dispersive spectroscopy (EDS) and microdiffraction revealed that the Ag formed 20–30 nm crystallites within a Bi-2212 matrix. Silver could not be found in the glass matrix within the resolution of the EDS. Given the small weight fraction and fine crystallite size of the Ag, it is not surprising that the Ag lines are not obvious in the XRD pattern.

Texture Apparatus

The texturing apparatus is described elsewhere.[8] Briefly, the sample to be textured is compressed between two high-density Al_2O_3 rods contained within an alumina tube that allows the atmosphere around the sample to be controlled throughout the process. The tube is surrounded by a three-zone furnace which minimizes the thermal gradients around the sample. The furnace is programmed in all cases to ramp to a specified temperature at 10°C per min.

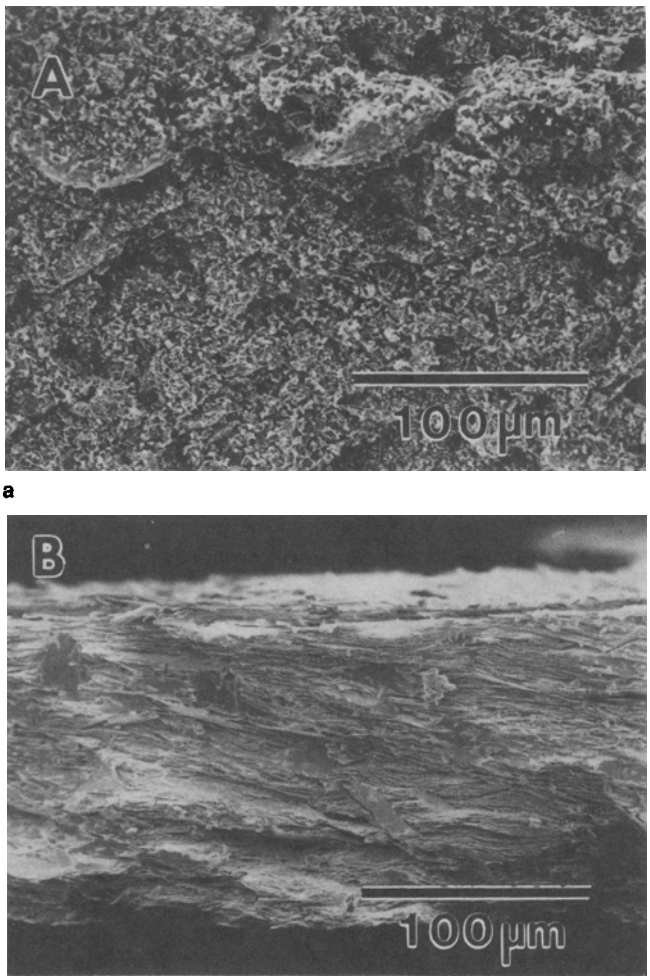

Fig. 2. Scanning electron micrcoscopy fracture micrographs of (a) amorphous BISCCO crystallized in the texture apparatus without an axial load, and (b) with a load (1500 N). Both samples crystallized at 870°C in a 20% oxygen, 80% argon.

Uniaxial force is generated by an electromotive drive that can maintain the load to within 1.2% of the set load. A linear displacement transducer is positioned to register the difference between the movement of the rods and the movement of the tube.

The micromilled powder, weighing between 150 and 165 mg is pressed into a 9.525 mm diameter pellet having a thickness of 0.5 mm and a green density of 4.8 grams/cc. The wafer is sandwiched between 0.125 mm thick Au foil and then placed between the alumina rods which have been coated on the ends with a thin layer of boron nitride to minimize friction and adhesion of the interface. The rods with the sample are placed in the alumina tube which is then flushed with > 100 cc/min of 20% oxygen-80% argon or nitro-

gen gas mixture for at least 10 min. The flow rate is reduced to 50 cc/min during the texturing run. The electromotive drive is activated to preload the system with a force of 250 N. The furnace is ramped to temperature while the sample is loaded to 1500 N. At the end of the texturing run, the power to the furnace is shut off and the furnace is opened to quench the sample. The sample cools to below 600°C in approximately 1 min. Dense, well textured samples are obtained with an applied load while a finer grained, porous and randomly oriented sample forms under identical conditions without the uniaxial load (Fig. 2).

RESULTS

Differential Thermal Analysis

Differential thermal analysis (DTA) was performed in atmospheres of 0, 10, 20, and 100% oxygen in nitrogen on powder samples of the as dropped spheres and fibers. For consistency, all measurements were taken in a flowing atmosphere at the rate of 50 cc/min at a constant heating rate of 10°C/min. Examination of the thermal events revealed systematic variations with both oxygen partial pressure and Ag content. The onset of melting decreased with decreasing oxygen partial pressure (Figs. 3 and 4) regardless of the Ag content. In addition, the Ag added material showed a marked decrease in the melting temperature with respect to the Ag free material, although this became less severe at lower oxygen partial pressures. Specifically, the onset of melting ranged from 853°C at a P_{O2} of 100% to 753°C at P_{O2} of 0% for the Ag added material, a significant decrease from the range of 888 to 774°C for the Ag-free material. In both samples, the first exotherm remained relatively static at approximately 460°C regardless of oxygen partial pressure. It seems that this first crystallization event is uneffected by either Ag addition or oxygen partial pressure. The second exotherm at approximately 500°C for the Ag-free material and 485°C for the Ag added material showed a systematic decrease in amplitude with decreasing oxygen partial pressure, disappearing in the absence of oxygen, for both materials. Both samples showed a small endotherm which occurred only in 100% oxygen. Unlike the other thermal events, though, the addition of Ag showed an increase in the onset temperature from 716°C in the Ag-added material to 687°C in the Ag-free material. The exact nature of this event is presently unknown,

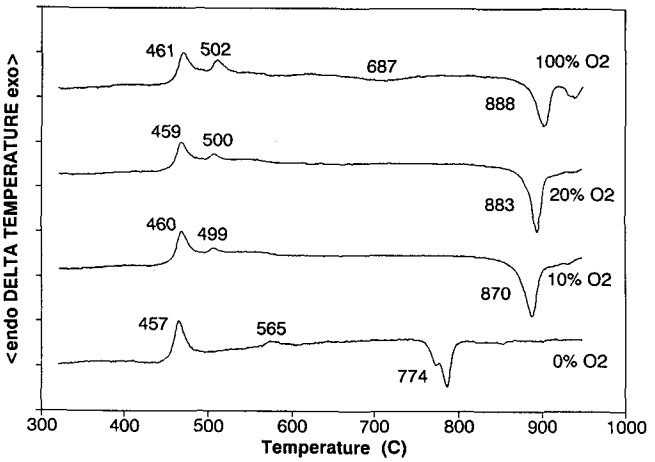

Fig. 3. Differential thermal analysis on the as-quenched BISCCO (Fig. 1) for various P_{O2}.

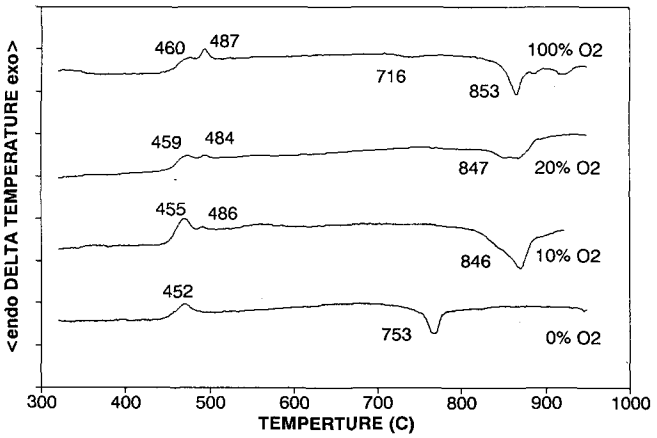

Fig. 4. Differential thermal anlaysis on the gas jet fibers of BISCCO + Ag (Fig. 1) for various P_{O2}.

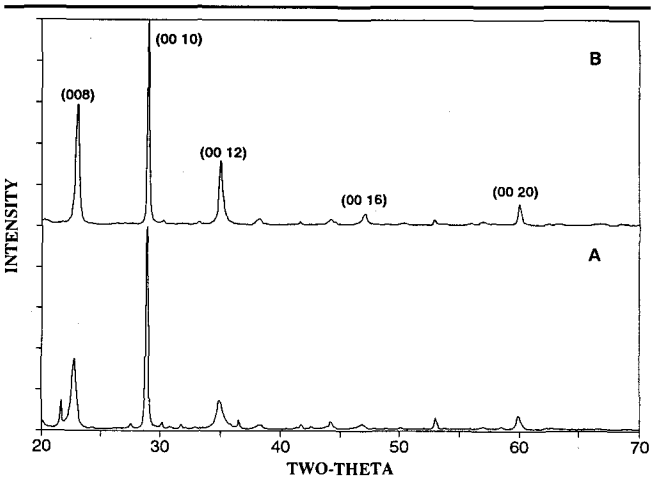

Fig. 5. X-ray diffraction, using $Cu_{k\alpha}$, of the surface of the (a) BISCCO textured at 880°C, and (b) annealed for 72 h at 850°C.

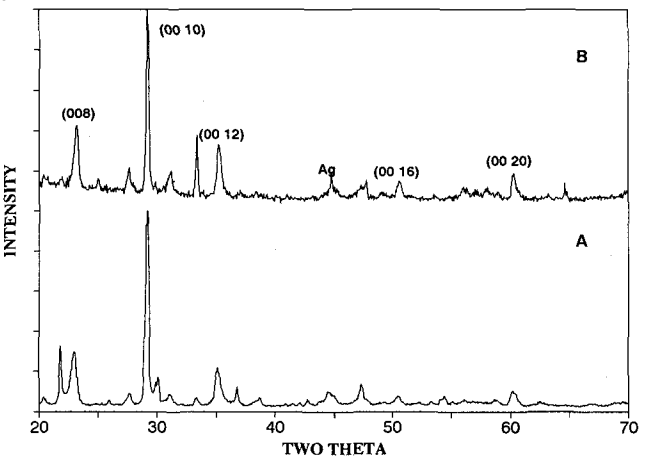

Fig. 6. X-ray diffraction, using $Cu_{k\alpha}$, of the surface of the BISCCO + Ag (a) textured at 850°C and (b) annealed for 86 h at 850°C.

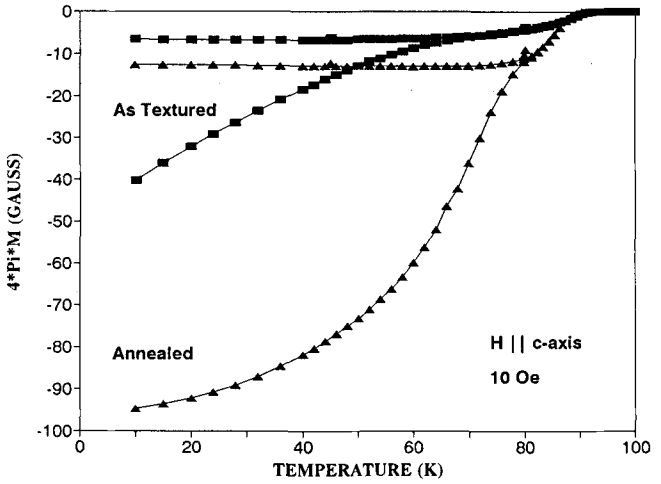

Fig. 7. DC magnetization as a function of temperature at 10 Oe for H || c-axis of the as-textured BISCCO and annealed samples shown in Fig. 5.

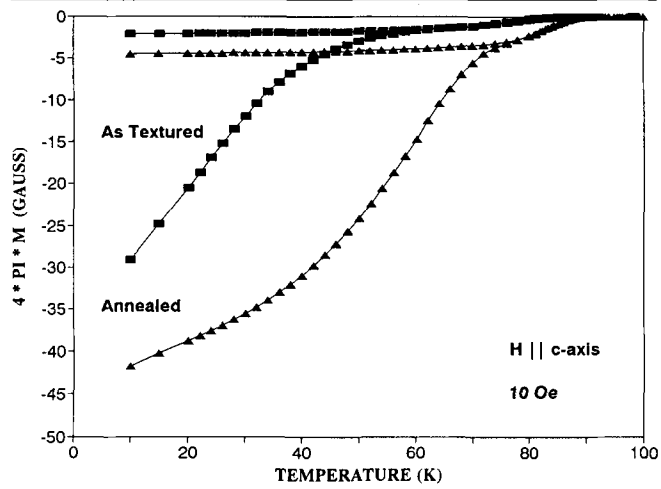

Fig. 8. DC magnetization as a function of temperature at 10 Oe for H || c-axis of the as-textured BISCCO + Ag and annealed samples shown in Fig. 6.

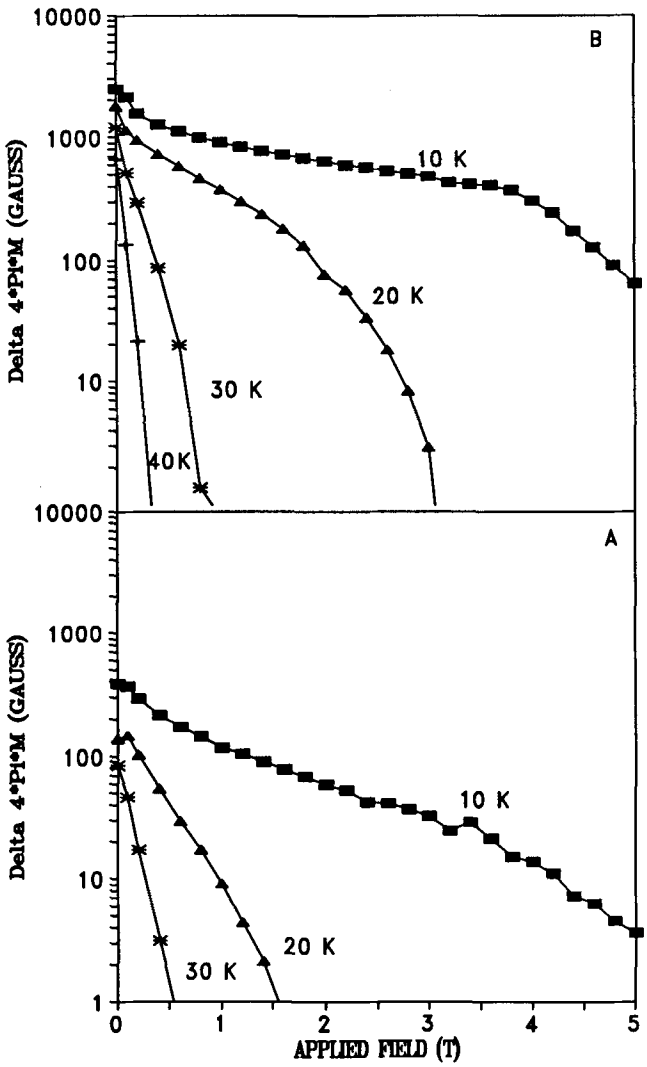

Fig. 9. $\Delta 4\pi M$ up to 5 T at various temperatures for (a) as-textured, and (b) annealed samples shown in Fig. 7.

but its existence does suggest the need to process at lower oxygen partial pressures. In order to enhance crystal growth kinetics yet minimize second phase formation, all heat treatments were performed in 20% oxygen, 80% argon or nitrogen.

Texturing

It has been shown that the best texture development occurs within a few degrees of the onset of melting.[8] Two samples will be compared. A sample without Ag heated to 880°C and 1500 N for 4 h and another with Ag added heated to 850°C and heated for 20 h. Both samples show good textured based upon the enhancement of the (00l) lines over all other lines but the Ag-added material shows more non-(001) lines (Figs. 5a and 6a). Characteristic to both the as-textured samples is the broadening of the lines and the sharp (006) line of the Bi-2201. In addition, there are nonsystematic shifts in the (001) peak positions. By annealing the samples in 20% oxygen for > 60 h, the (006) could be eliminated, the (001) peaks sharpened considerably, and the (001) lines shift closer to their theoretical positions. No appreciable grain growth appears to have occurred during annealing. Grains range from 20 to 40 μm along the basal plane direction and 0.5 to 2 μm in the c-axis direction based on TEM analysis.

Superconducting Properties

DC SQUID magnetization was used to quantify the superconducting properties of these materials. Of critical importance is how phase purity and degree of texture effect the weak-link behavior in these materials.

Characteristic to both the Bi-2212 and Bi-2212 + Ag as-textured materials is a superconducting transition (T_c) of 90K, a consistent Meissners fraction with a sharp transition and a broad zero-field cooled (ZFC) superconducting transition. The extremely broad ZFC transitions suggests that these samples are comprised of weak-linked regions which have a wide range of critical currents. With annealing, the ZFC

transitions sharpen and the magnitude of the diamagnetic screening increases more than a factor of two for the Bi-2212 and by 50% for the Bi-2212+Ag (Figs. 7 and 8).

Hysteresis loops provide an indirect measure of the current carrying capacity (J_c). The as-textured sample show modest field dependence for 10K, and an increasing field dependence as temperature increases (Fig. 9). Annealing increases the width of the hystersis loops by nearly a factor of 5 while decreasing the field dependence. Given the weak-linked behavior of these materials, annealing appears to improve the intracrystalline J_c of these materials. However, removing too many of the intercalations could have a detrimental effect on J_c since defects associated with the intercalations could help to improve flux pinning.

DISCUSSION

The crystallization path for amorphous BISCCO with and without Ag changes with P_{O2}. The onset of melting decreases with decreasing P_{O2} but the onset of crystallization remains the same. However, the second exotherm decreases with decreasing P_{O2}. The addition of Ag alters the crystallization and lowers the melting temperature. It has been demonstrated that the first exotherm is associated with the formation of the Bi-2201 phase while the second exotherm is associated with the formation of alkali-cuprates.[9] The endotherm at 687°C in pure oxygen has been attributed to the formation of the Bi-2212,[10] but this has not been substantiated by heating and quenching experiments,[9] or with high temperature XRD. Most recent work concludes that the formation of the Bi-2212 from the Bi-2201 is via intercalation of the Sr-Ca-Cu-O species and is diffusion limited.[9,10] This could be problematic for the Ag-added material since it must be processed at a lower temperature to avoid melting. The previous study showed that the texturing occurs during the grain growth stage. Tracer diffusion studies have shown that diffusivity of oxygen is orders of magnitude faster in the basal plane than in the c-axis direction,[13] hence it is likely that cation diffusion will be faster in the basal plane also. If the Bi-2201 undergoes considerable textured growth (> 10 μm) prior to intercalation, the distance the Sr-Ca-Cu-O must diffusive relative to the finer more randomly distributed grains is greater, resulting in slower rate of intercalation.

Transmission electron microscopy shows in detail what is suggested by XRD and DC SQUID, that the Bi-2212 is not completely formed in the as-textured material (Fig. 10). Numerous Bi-2201 layers of various widths can be readily seen in this lattice image. Hendricks and Teller[14] provide an analytical technique for determining the number of intercalations in partially ordered layered structures based upon shifts in peak positions and line broadening in XRD. This model predicts the nonsystematic peak shifts and broadening observed, unlike the simple strain model where a uniform strain results in a systematic shift in peak positions. The number of intercalations are varied till the model peak shifts best fit the measured shifts and peak broadening (Table I). This technique has also been applied to determine the number of Bi-2212 layers in Bi-2223.[15] The Bi-2212 as-textured has fewer intercalations and a higher proportion are eliminated with annealing than the Ag-added material. It

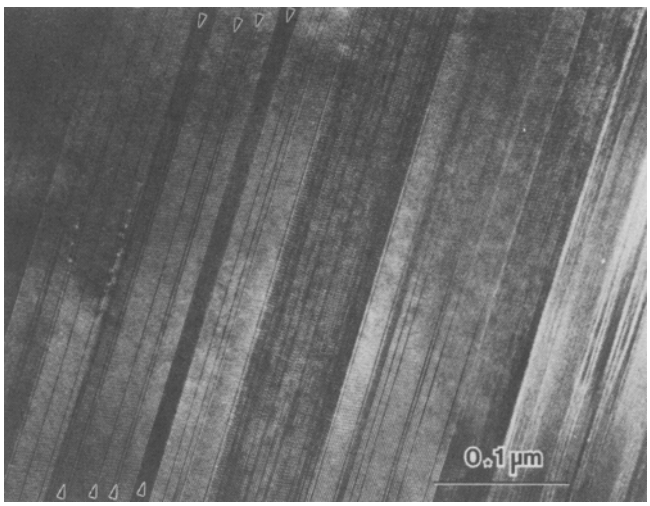

Fig. 10. Transmission electron microscopy low resolution lattice image showing the variations in lattice spacings across a grain. The arrows indicate some of the Bi-2201 layers in the dominantly Bi-2212 matrix.

Table I. Best Fits for Shifts in Two-Theta Peak Positions (Δ2θ) and Peak Broadening (FWHM) for a Given Percent Bi-2201 Intercalations (%) in Bi-2212

	Bi-2212						Bi-2212+Ag					
	As-Textured			Annealed			As Textured			Annealed		
HKL	Δ2θ	FWHM	%	Δ2θ	FWHM	%	Δ2θ	FWHM	%	Δ2θ	FWHM	%
0 0 8	–0.111	0.209	20	–0.032	0.103	5	–0.145	0.259	30	–0.088	0.080	15
0 0 10	0.074	0.105	15	0.027	0.118	5	0.121	0.205	30	0.052	0.104	10
0 0 12	0.116	0.519	20	0.043	0.241	5	0.191	0.908	30	0.082	0.381	10
0 0 16	–0.160	0.375	20	–0.048	0.196	5	*	*	*	*	*	*
0 0 20	0.100	0.259	12	0.048	0.167	5	0.198	0.482	30	0.085	0.133	10

*Interference from non-(00l) lines.
Note: Using c-axis lattice parameters of 3.093 and 2.462 nm for Bi-2212 and Bi-2201, respectively, based on Hendricks' and Teller model.[14]

is still unclear whether the incomplete formation of the Bi-2212 + Ag material is due to lower diffusivity due to lower temperatures or if the Ag acts to inhibit diffusion of the Sr-Ca-Cu-O. X-ray diffraction demonstrates that some coarsening of the Ag occurs during texturing. More work is being carried out to determine the effect of Ag on the formation of the Bi-2212.

CONCLUSIONS

It has been demonstrated that well textured Bi-2212 can be formed by crystallizing an amorphous precursor with or without Ag under a uniaxial stress by heating to within 99% of the melting temperature. However, the resulting Bi-2212 is heavily intercalated with Bi-2201. These intercalations can be removed by annealing at high temperatures for long times. The intracrystalline J_c improve with annealing. However, the optimal number of intercalations has yet to be determined. Silver and P_{O2} both effect the crystallization pathway in a yet to be determined manner. Silver-added material shows promise in enhancing the strain tolerance[16] but also results in lower diffusion rates of the Sr-Ca-Cu-O to form the Bi-2212 from the Bi-2201. Altering either the P_{O2} or composition may enhance the reaction kinetics. These possibilities are being explored.

ACKNOWLEDGMENTS

We would like to thank Kevin Dennis for his assistance in this project and R.A. Gleixner of Babcock and Wilcox for providing the amorphous BISCCO fibers in this work. The work was performed at Ames Laboratory, Iowa State University, and supported by the Director of Energy Research, Office of Basic Sciences, U.S. Department of Energy under Contract No. W-7405-ENG-82 and at Argonne National Laboratory under National Science Foundation grant DMR-88-09854.

REFERENCES

1. S. Jin, R.B. van Dover, T.H. Tiefel, J.E. Graebner and N.D. Spencer, *Appl. Phys. Lett.* 58, 868 (1991).
2. B.M. Moon, G. Kordas, M.R. Teepe, D.S. Kenzer, Y.L. Jeng and D.L. Johnson, *Proc. Second Intl. Conf. on Electronic Material (ICEM'90),* ed. N. Chimsky, (Pittsburgh, PA: Materials Research Society, 1990) pp. 39–44.
3. K. Heine, J. Tenbrink and M. Thoner, *Appl. Phys. Lett.* 55, 2441 (1989).
4. K.H. Sandhage, G.N. Riley, Jr. and W.L. Carter, *JOM* 43, 21 (1991).
5. N. Enomoto, H. Kikuchi, N. Uno, H. Kumakura, K. Togano and K. Watanabe, *Jpn. J. Appl. Phys.* 29, L447 (1990).
6. Y. Yamada, K. Jikihara, T. Hasebe, T. Yanagiya, S. Yasuhara, M. Ishihara, T. Asano and Y. Tanaka, *Jpn. J. Appl. Phys.* 29, L456 (1990).
7. M. Yoshimura, T.-H. Sung, Zenbe-e Nakagawa and T. Nakamura, *Jpn. J. Appl. Phys.* 27, L1877 (1988).
8. S.R. Arrasmith, M.J. Kramer, B.D. Merkle, T.G. Holesinger and R.W. McCallum, *J. Mat. Res.* 8, 1247 (1993).
9. G. Holesinger, D.J. Miller and L.S. Chumbley, *J. Mat. Res.* 7, 1658 (1992).
10. D.P. Matheis, S.T. Misture and R.L. Snyder, *Physica C* 207, 134 (1993).
11. R.W. McCallum, M.J, Kramer, T.J. Folkerts, S.R. Arrasmith, B.D. Merkle, S.I. Yoo, Y. Xu and K.W. Dennis, *Oxide Superconductors,* eds. S.K. Malik and S.S. Shah (in press).
12. S.E. LeBeau, J. Righi, J. Ostenson, S.C. Sanders and D.K. Finnemore, *Appl. Phys. Lett.* 55, 292 (1989).
13. M. Runde, J.L. Routbort, S.J. Rothman, K.C. Goretta, J.N. Mundy, X. Xu and J.E. Baker, *Phys. Rev. B* 45, 7375 (1992).
14. S. Hendricks and E. Teller, *J. Chem. Phys.* 10, 147 (1942).
15. J.M. Tarascon, W.R. McKinnon, P. Barboux, D.M. Hwang, B.G. Bagley, L.H. Greene, G.W. Hull, Y. LePage, N. Stoffel and M. Giroud, *Phys. Rev. B* 38, 8885 (1988).
16. K. Togano, H. Kumakura, J. Kase, Q. Li, J.E. Ostenson and D.K. Finnemore, *J. Appl. Phys.* 70, 6966 (1991).